

## Computational Modeling Toward Understanding Agonist Binding on Dopamine 3

Yaxue Zhao,<sup>†,§</sup> Xuefeng Lu,<sup>||</sup> Chao-yie Yang,<sup>⊥</sup> Zhimin Huang,<sup>†</sup> Wei Fu,<sup>#</sup> Tingjun Hou,<sup>\*,‡</sup> and Jian Zhang<sup>\*,†</sup>

Department of Pathophysiology, Key Laboratory of Cell Differentiation and Apoptosis of Chinese Ministry of Education, School of Medicine, Shanghai Jiao Tong University, Shanghai 200025, China, Functional Nano & Soft Materials Laboratory (FUNSOM) and Jiangsu Key Laboratory for Carbon-Based Functional Materials & Devices, Soochow University, Suzhou, Jiangsu 215123, China, School of Pharmacy, Shanghai Jiao Tong University, 800 Dongchuan Road, Shanghai 200240, China, Section of Molecular Biology, Division of Biological Sciences, University of California, San Diego, 9500 Gilman Drive, La Jolla, California 92093, Departments of Internal Medicine, Pharmacology, and Medicinal Chemistry, Comprehensive Cancer Center, and Center for Computational Medicine and Bioinformatics, University of Michigan, 1500 East Medical Center Drive, Ann Arbor, Michigan 48109, and Department of Medicinal Chemistry, School of Pharmacy, Fudan University, Shanghai 201203, China

Received May 27, 2010

The dopamine 3 (D3) receptor is a promising therapeutic target for the treatment of nervous system disorders, such as Parkinson's disease, and current research interests primarily focus on the discovery/design of potent D3 agonists. Herein, a well-designed computational protocol, which combines pharmacophore identification, homology modeling, molecular docking, and molecular dynamics (MD) simulations, was employed to understand the agonist binding on D3 aiming to provide insights into the development of novel potent D3 agonists. We (1) identified the chemical features required in effective D3 agonists by pharmacophore modeling based upon 18 known diverse D3 agonists; (2) constructed the three-dimensional (3D) structure of D3 based on homology modeling and the pharmacophore hypothesis; (3) identified the binding modes of the agonists to D3 by the correlation between the predicted binding free energies and the experimental values; and (4) investigated the induced fit of D3 upon agonist binding through MD simulations. The pharmacophore models of the D3 agonists and the 3D structure of D3 can be used for either ligand- or receptor-based drug design. Furthermore, the MD simulations further give the insight that the long and flexible EL2 acts as a "door" for agonist binding, and the "ionic lock" at the bottom of TM3 and TM6 is essential to transduce the activation signal.

### INTRODUCTION

The studies on the dopamine 3 (D3) receptor, discovered by Sokoloff and co-workers 15 years ago, have made enormous progress, which improves our understanding of its physiological and pharmacological impact significantly.<sup>1</sup> Compared to the D1 and D2 receptors, the D3 receptor is much less abundant and concentrated almost exclusively in limbic brain regions, such as the nucleus accumbens, olfactory tubercle, and islands of Calleja.<sup>2–4</sup> Recent studies have suggested that the D3 receptor contributes to the beneficial influence of dopaminergic agonists for the protection and restoration of the dopaminergic pathways in Parkinson's disease.<sup>5</sup> The D3 receptor is therefore considered to be a promising therapeutic target for the treatment of such

disorders, and there is strong research interest in the design of potent D3 agonists.<sup>6–8</sup>

Accurate three-dimensional (3D) structures for the dopamine receptors are not available, and the structural basis of the agonist binding to the D3 receptor is poorly understood. Considerable efforts were made for the prediction of the D3 structure based on a distal G-protein coupled receptor (GPCR) family protein, rhodopsin,<sup>9</sup> as the template, which has less than 30% sequence similarity to D3. We have found several moderate potent ligands of the D3 receptor based on homology model from the rhodopsin template.<sup>10</sup> However, the structure information of D3 based on a low-homologous template is a significant impediment to the rational design of highly potent D3 agonists. Recently, the crystal structures for the human  $\beta 2$  adrenergic ( $\beta 2$ AD) GPCR were solved.<sup>11,12</sup> The  $\beta 2$ AD and human dopamine receptors belong to the same subfamily of GPCR with more than 37% sequence similarity.<sup>13</sup> Therefore,  $\beta 2$ AD can be used as a better template to construct a more accurate model of the D3 receptor for studying the interactions between the D3 receptor and its agonists.

In the present work, we performed a computational study to investigate the agonist binding to the D3 receptor, which is important for rationally designing potent agonists of the D3 receptor. First, we analyzed the chemical features of D3

\* Corresponding authors. E-mail: jian.zhang@sjtu.edu.cn (J.Z.), tjhous@suda.edu.cn or tingjunhou@hotmail.com (T.H.). Telephone: +86-21-63846590-776922 (J.Z.), +86-512-65882039 (T.H.).

<sup>†</sup> School of Medicine, Shanghai Jiao Tong University.

<sup>‡</sup> Functional Nano & Soft Materials Laboratory (FUNSOM) and Jiangsu Key Laboratory for Carbon-Based Functional Materials & Devices, Soochow University.

<sup>§</sup> School of Pharmacy, Shanghai Jiao Tong University.

<sup>||</sup> Division of Biological Sciences, University of California, San Diego.

<sup>⊥</sup> Departments of Internal Medicine, Pharmacology, and Medicinal Chemistry, Comprehensive Cancer Center, and Center for Computational Medicine and Bioinformatics, University of Michigan.

<sup>#</sup> School of Pharmacy, Fudan University.

**Table 1.** Output of the Score Hypothesis Process on the D3 Agonist/Partial Agonist Set

compound	experimental $K_i$ (nm)	estimated $K_i$ (nm)	error factor <sup>a</sup>	mapped features			
				PI	HD	HY1	HY2
1	26	28	1.1	+	+	-	-
2	53	12	-4.5	+	-	+	+
3	0.18	0.12	-1.5	+	+	+	+
4	2000	210	-9.5	+	+	-	-
5	38	100	2.7	+	+	+	-
6	5.6	15	2.7	+	-	+	+
7	0.23	0.84	3.6	+	-	+	+
8	0.5	0.48	-1.0	+	-	+	+
9	3.2	2.7	-1.2	+	-	+	+
10	1.4	3.1	2.2	+	+	+	-
11	5.5	7.1	1.3	+	+	+	-
12	43	500	12	+	+	-	-
13	0.78	1.7	2.2	+	+	+	-
14	3.4	2.4	-1.4	+	+	+	-
15	0.57	2.6	4.6	+	+	+	-
16	69	26	-2.7	+	+	+	-
17	42	4.9	-8.6	+	+	+	-
18	10	2.8	-3.6	+	+	+	-

<sup>a</sup> Error factor is computed as the ratio of the measured activity to the activity estimated by the hypothesis or the inverse if estimated is greater than measured.

agonists by pharmacophore modeling. Subsequently, the 3D structure of the D3 receptor was built by homology modeling based on the template of the X-ray crystal structure of the human  $\beta$ 2AD receptor, and the ligand–receptor complex was then generated by docking method. Finally, molecular dynamics (MD) simulations were performed on the ligand-free D3 and an agonist-bound D3 to investigate the induced fit effect of the D3 receptor upon agonist binding.

## EXPERIMENTAL METHODS

**Agonist Pharmacophore Modeling.** A set of 18 different compounds, belonging to different structural classes of D3 agonists and partial agonists (Figure S1 in Supporting Information), were collected from different literatures.<sup>7,14–25</sup> The studied compounds have significant structural diversity and wide coverage of molecular bioactivities in terms of  $K_i$  ranging from 0.18 to 2000 nM (Table 1).

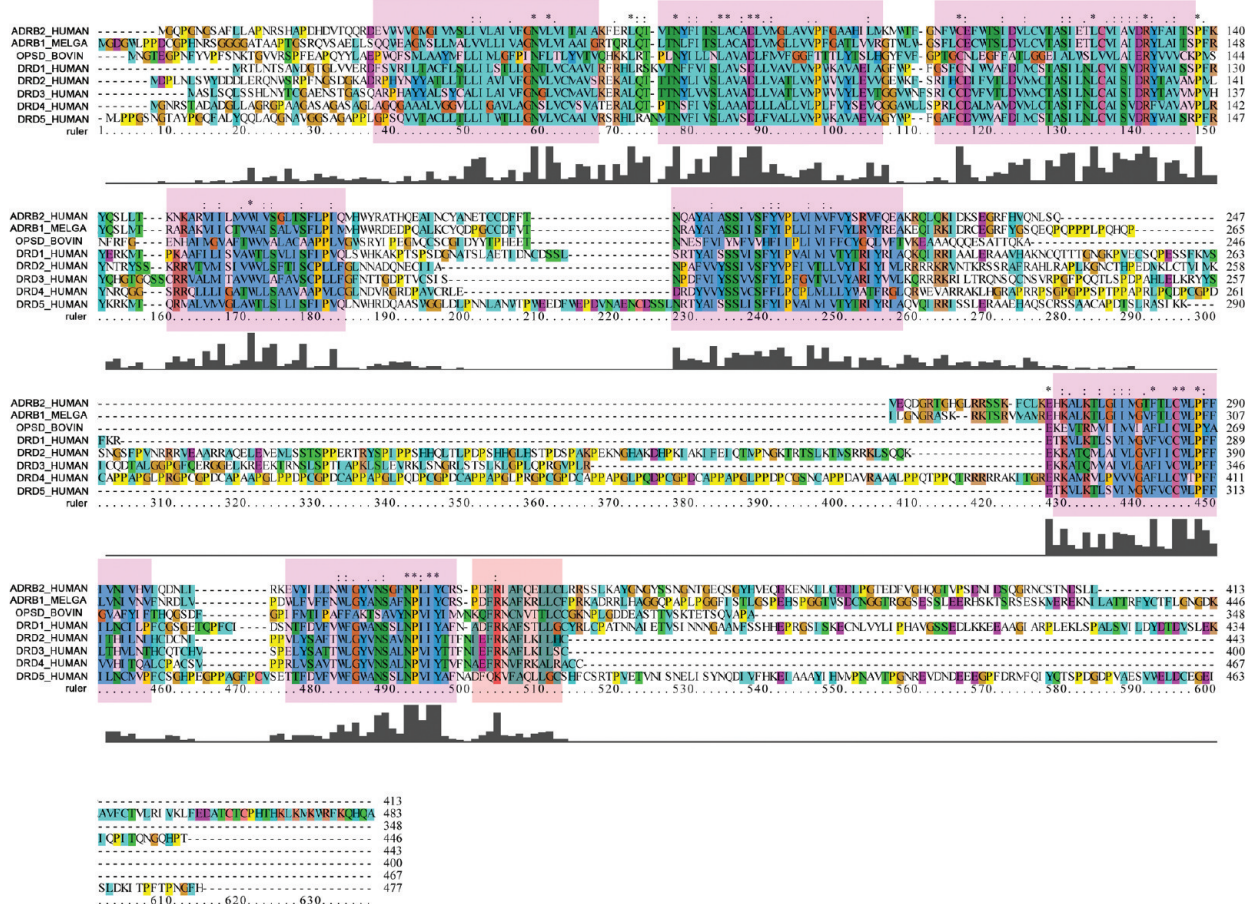
The compounds were built using Catalyst 2D-3D sketcher in Discovery Studio,<sup>26</sup> and a family of representative conformations were generated for each compound using the best conformational analysis method with the Poling algorithm<sup>27</sup> and the CHARMM force field.<sup>28</sup> A maximum number of 250 conformations of each compound were selected using the best conformer generation option with a constraint of 20 kcal/mol energy thresholds above the global energy minimum to ensure maximum coverage of the conformational space. Based on the conformations for each compound, the Catalyst Hypogen module<sup>29</sup> was employed to construct possible pharmacophore models. When generating a hypothesis, Catalyst attempts to minimize a cost function consisting of two terms. One penalizes the deviation between the estimated activities of the training set molecules and their experimental values, and the other penalizes the complexity of the hypothesis. Analysis of the functional groups on each compound in the training set revealed that four chemical features, including hydrogen-bond acceptor

and donor, hydrophobic group, and positive ionized point, were enough to map all of the critical chemical features. Exclude volume was also used to detect the space occupation feature from the D3 receptor. Hence, the five features were selected to represent the essential information in this hypothesis generation process.

**Homology Modeling.** The X-ray crystal structure of the human  $\beta$ 2AD receptor (PDB entry: 2RH1, resolution 2.4 Å)<sup>11,12</sup> was used as the template to construct the human D3 receptor. The sequence of the human D3 was retrieved from GenBank (P35462) (<http://www.uniprot.org/uniprot/>). The sequences of human D3 and  $\beta$ 2AD were aligned based on the sequence analysis of 493 members of the amine subfamily of GPCR proteins (Figure 1A). According to the secondary structure information of the template, the sequence alignment was adjusted manually to obtain a more reasonable alignment. Then, a 3D model of the human D3 receptor was generated using the program Modeller (version 9v2).<sup>30</sup> A total of 100 models were yielded, and each of them had three diverse optimized loop structures. All the modeled structures were checked by the Ramachandran plot and the substituted cysteine-accessibility method (SCAM).<sup>31</sup> The D3 models with more than four residues in the disallowed region of the Ramachandran plot or the wrong cysteine position in SCAM were filtered out, and the rest were maintained to match the pharmacophore hypothesis.

**Pharmacophore-Based Homology Model Selection.** The remaining homology models after the Ramachandran plot and the SCAM filters were checked one by one. The physiochemical properties of the residues in the binding pocket were used to match with the agonist pharmacophore model. The pair of Asp110 in the D3 model and the positive ionizable point in the pharmacophore model were positioned as the starting point, and then a comparison of the distance constraint between any two features in the pharmacophore model and the length of the corresponding physiochemical residue pairs was iteratively measured in the binding pocket of each homology model. Finally, the homology D3 candidate that satisfied the pharmacophore model best was identified as the agonist binding D3 receptor model.

**Construction for the 3D Model of D3-Compound 19 Complex.** The docking program GOLD<sup>32</sup> and scoring function X-Score<sup>33</sup> were applied to construct the D3–agonist complexes using the final homology model of D3 and a series of analogue compounds we studied before.<sup>22</sup> The center of the binding site for the D3 receptor was set at the center of Asp110 with a radius of 13 Å, large enough to cover the binding pocket. For each genetic algorithm (GA) run, a maximum number of 200 000 operations were performed on a population of 5 islands of 100 individuals. Operator weights for crossover, mutation, and migration were set to 95, 95, and 10, respectively. GoldScore implemented in GOLD was used as the primary scoring function to evaluate the docked conformations. The three highest ranked conformations for each compound were selected to be submitted to advanced binding energy calculation. Cheng et al. indicated that the success rate of docked ligand poses found within 2 Å of their crystal structures significantly increases to ~90% if the top three best-scored poses from GOLD are considered.<sup>34</sup> Therefore, all 27 binding poses of the 9 compounds, including pramipexole and its 8 analogues we designed in our previous study<sup>22</sup> (summarized in Table 2), with the D3



PHI

A

PSI

C

B

**Figure 1.** (A) Sequence alignment of the amine subfamily of the GPCR proteins. (B) Ramachandran plot of the selected D3 model. The distribution of the D3 residues (black dots) were shown in color: most favorable (red), additional allowed (yellow), and generously allowed (light yellow) regions. (C) The SCAM result of the selected D3 model. The cysteine residues were shown in sphere, and the solvent-exposed cysteine residue was labeled in black.

receptor were then predicted using X-Score v1.2, and the pose within the best linear correlation between the predicted binding free energy and the experimental value was chosen as the final pose in each compound.

**MD Simulations.** The MD simulations were performed using the GROMACS package version 3.3.1<sup>35</sup> with the GROMOS force field. The molecular topology file for compound 19 was generated by the program PRODRG.<sup>36</sup>

**Table 2.** Prediction of the Studied D3 Agonist/Partial Agonist Set by Docking to the D3 Model

compound <sup>a</sup>	experimental $\Delta G_{\text{bind}}$ (kcal/mol) <sup>b</sup>	estimated $\Delta G_{\text{bind}}$ (kcal/mol) <sup>c</sup>
13	-10.2	-10.1
19	-12.6	-13.9
20	-11.4	-11.7
21	-11.4	-12.0
22	-11.2	-10.9
23	-10.5	-10.7
24	-9.3	-9.4
25	-9.9	-9.5
26	-11.3	-11.0

<sup>a</sup> All compounds in the test set tested in our lab.<sup>22</sup> <sup>b</sup> Experimental binding energy was calculated by the following equation:  $\Delta G = -RT \ln K_i$ . <sup>c</sup> Binding energy was estimated by X-Score.

The partial atomic charges of compound 19 were determined by using the CHelpG method<sup>37</sup> implemented in Gaussin98<sup>38</sup> at the level of HF/6-31G\*. Then the free D3 and D3–compound 19 complex were inserted into a 2-palmitoyl-2-oleoyl-sn-glycero-3-phosphatidylcholine (POPC) membrane<sup>39,40</sup> in a TIP3P water environment, respectively. At the end, the simulation system for the free D3 is totally composed of 236 lipid molecules and 6593 water molecules, and the D3–compound 19 system contains 236 lipid molecules and 6591 water molecules.

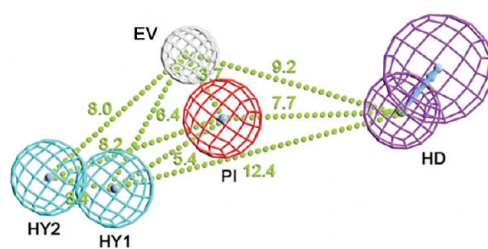
To maintain the system at a constant temperature of 300 K, the Berendsen thermostat<sup>41</sup> was applied using a coupling time of 0.1 ps. The pressure was maintained by coupling to a reference pressure of 1 bar. A coupling time of 1.0 ps was used for the simulations in bulk water.<sup>41</sup> The values of the isothermal compressibility were set to  $4.5 \times 10^{-5} \text{ bar}^{-1}$  for water simulations. All bond lengths involving hydrogen atoms were constrained by the LINCS algorithm.<sup>42</sup> Electrostatic interactions between charge groups at a distance less than 9 Å were calculated explicitly; long-range electrostatic interactions were calculated using the particle mesh Ewald (PME) algorithm<sup>43</sup> with a grid width of 1.2 Å and a fourth-order spline interpolation. A cutoff distance of 14 Å was applied for the Lennard-Jones interactions. The simulation cell was a rectangular periodic box, and the minimum distance between the protein, POPC, and the box walls was set to more than 8 Å so that the protein does not directly

interact with its own periodic image given the cutoff in every system. Numerical integration of the equations of motion used a time step of 2 fs with atomic coordinates saved every 10 ps. To neutralize the modeled systems, TIP3P water molecules were replaced by Cl<sup>-</sup> ions in the systems of both D3–POPC–TIP3P and D3–compound 19–POPC–TIP3P. These ions were located at positions of the chosen water oxygen atoms. All water molecules and ions in the simulation models were minimized with protein structures fixed by using the steepest descent method to the convergence criterion of 100 kJ/mol·nm, followed by energy minimizations on the whole systems. Water molecules, proteins, and POPC were coupled separately to a temperature bath at 300 K using a coupling time of 0.1 ps. Finally, 10 ns MD simulations were performed on both free D3 and D3–compound 19 systems.

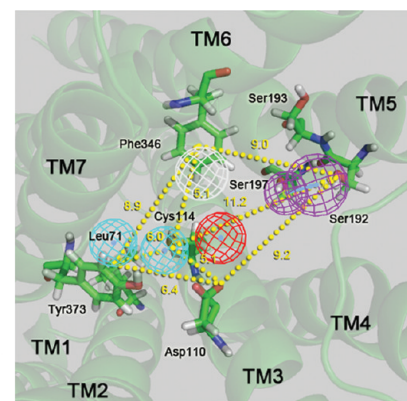
## RESULTS

**Pharmacophore Model of D3 Agonists.** The D3 receptor can bind both agonist and antagonist to induce different pharmacological effects, indicating the binding modes of agonist and antagonist in D3 receptor might be dissimilar.<sup>44</sup> To investigate the D3 agonist binding mode, the pharmacophore model of the D3 agonists was built to understand the key chemical features for agonist binding and further used as criteria to select a reasonable modeled D3 structure. The predictive pharmacophore model had five features as shown in Figure 2A: one positive ionized feature (PI), one hydrogen-bond donor feature (HD), one exclude volume feature (EV), and two hydrophobic points (HY1 and HY2), which were characterized by the highest cost difference, the lowest root-mean-square deviation (RMSD), and the best correlation coefficient (Figure S2 in Supporting Information). The results obtained from the pharmacophore model using the 18 diverse compounds were summarized in Table 1.

In the pharmacophore model, the features could be clustered into three parts in space. HD separated as one right part, covering rigid heterocyclic rings with polar substituents among the high-active compounds, i.e. —OH in dihydroxyphenyl and —NH in 4,5,6,7-tetrahydro-1H-indole, indicating that the residues involving the hydrogen-bond acceptor may locate on the right edge of the binding pocket of D3 and fix to the polar head of the D3 agonist. PI and EV formed the second part in the middle of the model. PI, associated with



A



B

**Figure 2.** (A) Generated pharmacophore model by Catalyst. Pharmacophore features were color coded with light-blue for hydrophobic groups (HY1 and HY2), red for positive ionized group (PI), magenta for hydrogen-bond donor (HD), and gray for exclude volume (EV). Distance between pharmacophore features is reported in angstroms. (B) Overlay of the pharmacophore and selected 3D structure models of the D3 receptor.

the protonated sp<sup>3</sup>-hybrid nitrogen, is the most significant character in D3 ligands. All compounds mapped the features in our model, and the compound without the protonated nitrogen barely bound to the D3 receptor.<sup>45</sup> EV had a 6.4 Å distance behind the PI feature, suggesting that the shape of the binding pocket of the D3 receptor is channel-like with a 5–8 Å width in the middle instead of sphere- or basin-like. The distance between the right and middle parts was 7–10 Å, providing the space arrangement of the effective polar residues in the D3 receptor. The third part was composed of HD1 and HD2, closing to each other and mapping most of the hydrophobic tails of the compounds, viz., aliphatic carbon and aliphatic and aromatic rings. Overall, the pharmacophore model revealed the key features of the agonist binding and drew the outline of the shape and feature distribution in the binding pocket of the pseudo-D3 receptor, which is in good agreement with a series of results from medicinal chemistry and QSAR studies.<sup>44–46</sup>

**Modeling of D3 Receptor and Validation.** The dopamine family and β2AD belong to the amine subfamily, which is parallel to the opsin subfamily of rhodopsin within the GPCR superfamily phylogenetic tree.<sup>13</sup> The basic structural topology and the sequence alignment of the dopamine family, β2AD, and rhodopsin are shown in Figure 1A, including the seven transmembrane helices (TM1–TM7), an additional short helical region (TM8) at the intracellular end of TM7, the three extracellular loops (EL1–EL3), and the three intracellular loops (IL1–IL3). The alignment analysis showed that β2AD shared ~37% full sequence identity with the D3 receptor, much higher than the identity between rhodopsin and D3 (~21%), especially on the consistency of the place of proline (Figure 1A), suggesting that β2AD could provide more accurate structural information to model the D3 receptor in comparison with the rhodopsin template. Therefore, we used the β2AD structure determined at 2.4 Å resolution<sup>11</sup> as the template to model the D3 receptor.

The β2AD structure is lacking the IL3 information because of its highly flexible disruption in crystallization. We are primarily interested in the ligand binding site of the D3 receptor, which is in the extracellular half of the TM region. Furthermore, interchanging the IL3 loop between the D2/D3 sequences in D2/D3 chimeras was found to have no effect on ligand binding affinities, suggesting that the long IL3 loop may not be crucial for ligand binding.<sup>47,48</sup> Therefore, the 3D structure models of the full-length D3, except IL3, were built and refined using Modeller in this study, and the generated models were verified by Ramachandran plot and SCAM.

Although the binding site of the D3 receptor has not been extensively studied, the binding site of the D2 receptor has been mapped using SCAM.<sup>31,49–55</sup> The sequence identity between the TM regions of D2 and D3, which includes the ligand binding site, is 80%. So it is understandable why many ligands have similar affinities when binding to the D2 and D3 receptors. The 3D structures of the binding sites in the D2 and D3 receptors should be similar, and the mapped binding site information for the D2 receptor should be applicable to that of the D3 receptor. Excluding bridging cysteine residues, there are two cysteine residues in the EL region and five cysteine residues in the TM region in the D2 receptor, corresponding to C355 and C358 and C51, C114, C122, C166, and C341 in the D3 receptor. In D2,

C118 which corresponds to C114 in the D3 receptor was shown to be the only cysteine residue exposed to solvent among these seven cysteine residues.<sup>51</sup> Accordingly, the built D3 models which were in agreement with the SCAM experiments and only possessed C114 exposed to solvent were considered to be the agonist-binding receptor candidates for the following calculations.

After being checked by Ramachandran plot and SCAM, 35 structures were validated as agonist-binding receptor candidates. Then they were compared with the above built pharmacophore hypothesis one by one, and the modeled D3 structure which can accord with the pharmacophore best (Figure 2B) was chosen for the following docking studies. Figure 1B and C showed the selected structure's Ramachandran plot and SCAM results, respectively. It can be found that all residues of the D3 receptor model fall in a reasonable area with 95.6% core, 4.0% allow, 0.4% general, and 0% disallow (see Figure 1B).

**Binding Mode of Compound 19 in D3 Receptor.** The pramipexole (compound 13 in Figure S1 in Supporting Information) and its analogues reported in our previous study<sup>22</sup> (Figure 3) were docked to D3 using GOLD<sup>32</sup> software, and their binding energies were predicted by X-Score. The experimental binding energies and the predicted values of these compounds listed in Table 2 showed a good linear correlation (Figure S3 in Supporting Information). That is to say, the homology model of the D3 receptor is reliable enough to produce the binding modes of pramipexole and its analogues in the binding site of the D3 receptor.

Among the series of the homologues shown in Figure 3, compound 19 with the strongest binding affinity with D3 was selected for the further MD simulations. The binding mode which can generate the best linear correlation was chosen to obtain a D3–agonist complex as a starting model for the following MD simulations. The D3 binding pocket was divided into three parts labeled A–C in Figure 4A by the three substituted groups in the center nitrogen atom of compound 19. As shown in Figure 4B, the protonated center nitrogen atom in compound 19 formed a salt bridge with the conserved negatively charged Asp110. The polar group in compound 19 inserted into the pocket A mainly interacted with D3 by hydrogen bonds. The thiazole ring not only formed hydrogen bonds with residues Ser192 and Ser193 but also made interactions with aromatic residues Phe345 and His349 of the D3 receptor. The *n*-propyl group of compound 19 had hydrophobic interactions with pocket B formed by residues Cys114, Val111, and Val107. The naphthal ring of compound 19 also had hydrophobic interaction with pocket C, including residues Tyr373, Phe338, Met113, Val78, and Leu71. Besides that, there was a hydrogen bond between the NH group of compound 19 and the residue Met113 of the D3 receptor.

Most of the D3 receptor residues involved in the interactions with compound 19 can be validated by experimental data. In fact, only sparse site-directed mutagenesis data concerning D3 exist to date. They are residues Cys114,<sup>56</sup> Ser192,<sup>57</sup> Ser193,<sup>57</sup> and His349.<sup>58</sup> Their mutations lead to various effects on ligand binding. However, some residues can be evidenced to be important based on the mutation data of the corresponding residues in the D2 receptor because of their high identity (the sequence identity is 80% between

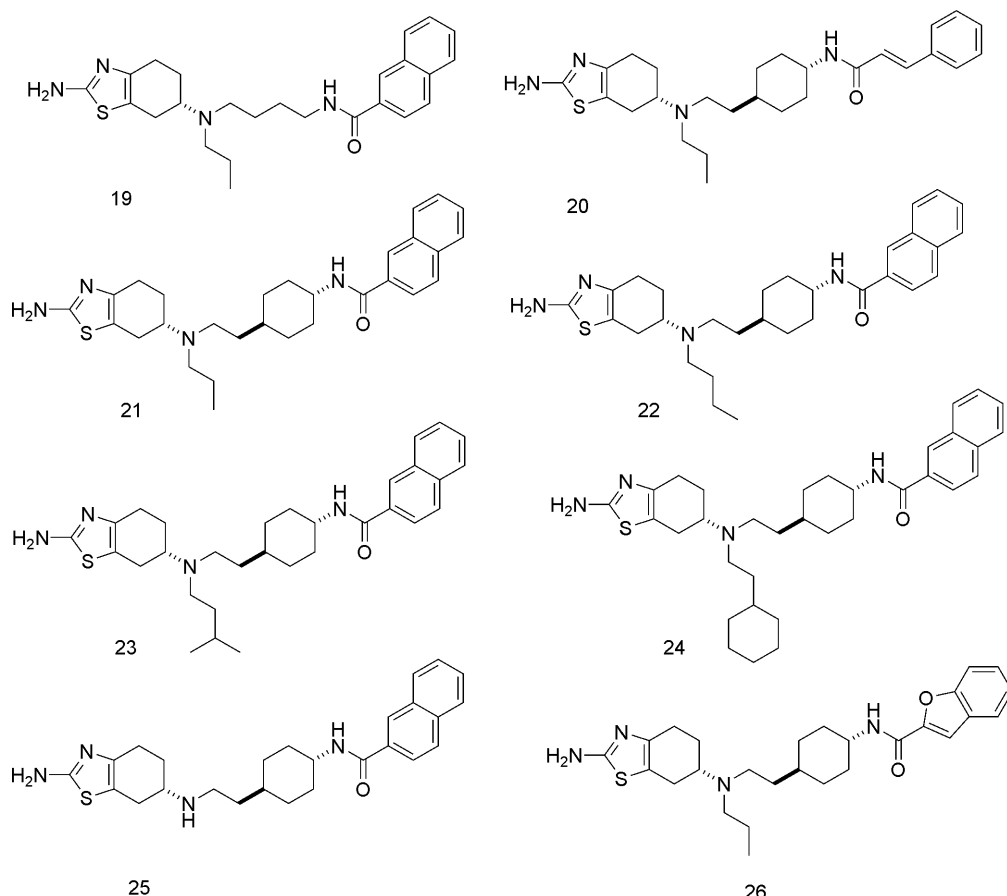


**Figure 3.** The 2D chemical structures of the 8 test set molecules from our lab.

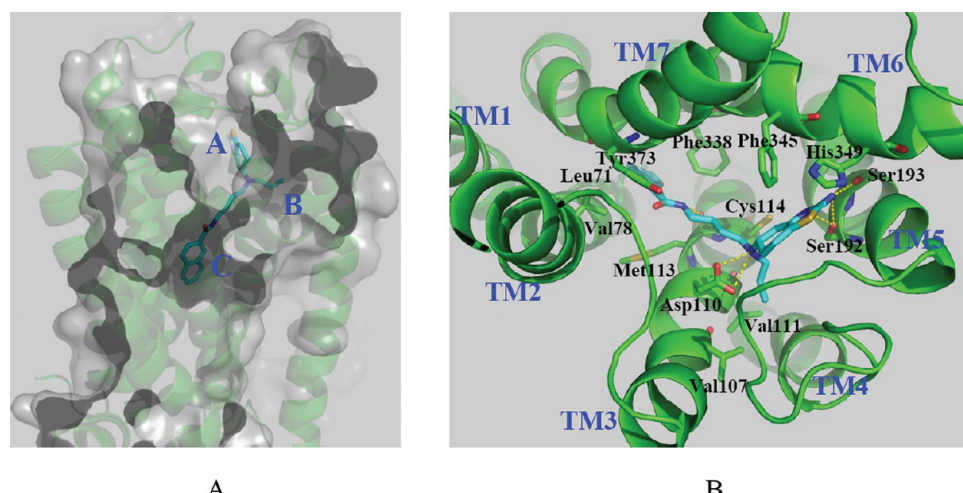


**Figure 4.** Binding mode of compound 19 in the D3 receptor. Compound 19 was shown in cyan stick, while D3 was shown in green cartoon. (A) Three binding pockets labeled in blue of compound 19. (B) Detailed interactions of compound 19 with the D3 receptor.

the TM regions of D2 and D3). Such residues include Asp110,<sup>59</sup> Val111,<sup>31</sup> Phe345,<sup>60</sup> and Tyr373.<sup>61</sup> Therefore, the binding mode of compound 19 in D3 is reasonable, and the complex can be used as a starting structure for investigating the agonist induced fit of the D3 receptor.

**D3 Dynamic Mechanism by Compound 19 Binding.** Both of the built system of D3–compound 19 and the free D3 system were submitted to the MD simulations with the following reasons: to investigate the active state structure of D3 and the inactive state structure of D3 and to recognize the agonist induced fit of D3 by comparing the two structures.

The 10 ns MD simulations were performed on both of the systems, and their RMSDs of the protein main chain atoms were monitored along the whole MD process. As shown in Figure S4 (Supporting Information), the RMSD value of the free D3 system (red line in Figure S4) was higher than that of the D3–compound 19 system (black line in Figure S4), indicating that the binding of the agonist stabilized the conformation of the D3 receptor. To examine the mobility of the D3 residues in free and bound states, the root-mean-square fluctuations (RMSFs) of the main chain atoms in the two systems were investigated (Figure S5 in

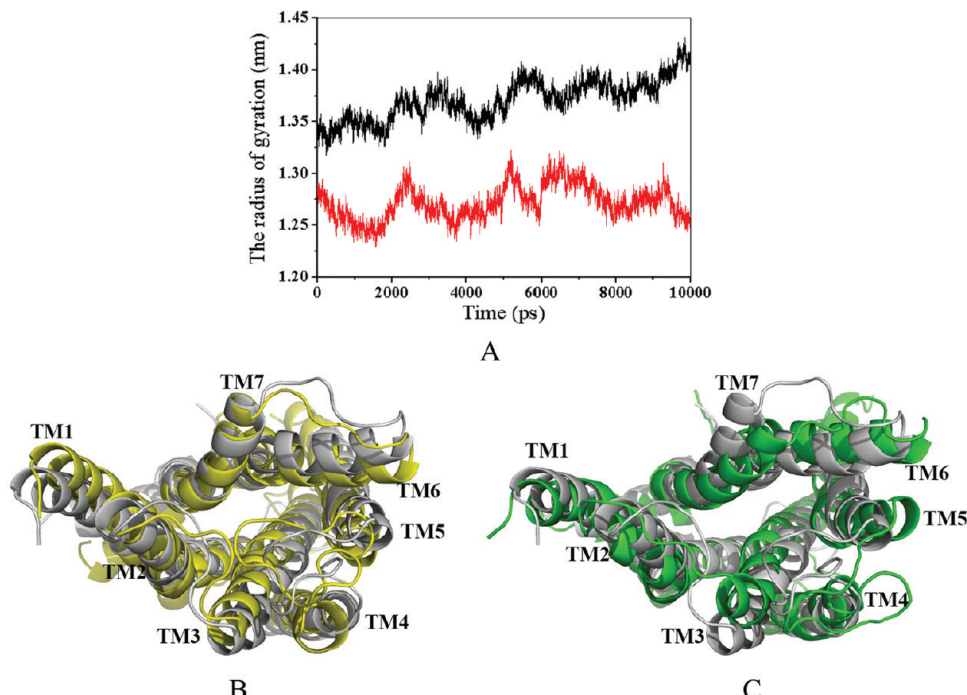


**Figure 5.** Time-dependent radius of gyration about the  $z$  axis of the D3 receptors in both free D3 (red line) and D3–compound 19 (black line) simulation systems. (B) Conformational comparison of the D3 receptors before (starting conformation in gray) and after (final conformation in yellow) the 10 ns MD simulation in the free D3 system. (C) Conformational comparison of the D3 receptors before (starting conformation in gray) and after (final conformation in green) the 10 ns MD simulation in the D3–compound 19 system. The D3 receptors are shown in cartoon, and transmembrane helices are labeled.

Supporting Information). The two systems had similar profiles in the RMSF distribution except for the region around residue 175. This region belonged to EL2 of the D3 receptor, and its much larger fluctuation in the free state (red line in Figure S5 in Supporting Information) than in the bound state (black line in Figure S5 in Supporting Information) might be the result of the agonistic effect.

The radii of gyration along the  $z$  axis of the two systems were also calculated to investigate the conformational rotary motion in membrane when D3 was activated by the agonist. Figure 5A showed that the radius of gyration of the bound state D3 was bigger by about 0.10 nm than that of the free state D3 during the 10 ns MD simulations. In other words, D3 had greater rotary motion in the membrane when it was bound by an agonist. The tendency could also be discovered by comparing the 10 ns D3 conformation with the starting D3 conformation in both systems (Figure 5B and C). It is obvious that the rotary degree between the active state D3 (green structure in Figure 5C, 10 ns D3 conformation in D3–compound 19 system) and the starting MD simulation D3 (gray structure in Figure 5) was larger than that between the free inactive state D3 (yellow structure in Figure 5B, 10 ns D3 conformation in free D3 system) and the starting MD simulation D3, especially for TM3 and TM7 which were reported mainly involved in ligand binding.<sup>45</sup> And maybe the activation of the D3 receptor by an agonist leads to the dramatic movement of TM3 and TM7.

To recognize the agonist induced fit effects of D3 in detail, the active (10 ns D3 conformation in D3–compound 19 system) and inactive (10 ns D3 conformation in free D3 system) D3 structures were compared. Two dramatic conformational changes were observed: one was in the outside of the membrane, and the other was in the inside of the membrane (Figure 6). Among the three extracellular loops,

EL2 was longest, and it was much more flexible in the free state than in the bound state during the MD simulations, which could be estimated by their RMSF values in Figure S5 in Supporting Information. As shown in Figure 6A, the long flexible EL2 had interaction with EL1 in the inactive state through residues Ser182 and Trp96. There was a hydrogen bond between the OH group in Ser182 and the carbonyl oxygen atom in Trp96. However, when D3 was activated by an agonist, the hydrogen bond disappeared (Figure 6B), and the distance between the two oxygen atoms increased nearly 10-fold. In the inside of the membrane, the “ionic lock” existing in the high-resolution structure of inactive rhodopsin<sup>62</sup> could also be found in the inactive D3 receptor (Figure 6C). In the inactive state D3, the Arg128 formed an “ionic lock” with Glu324 mediated by residue Tyr138. And the “ionic lock” interaction was disrupted when D3 was in the active state (Figure 6D), which is corresponding to the activated  $\beta$ 2AD.<sup>12</sup> Thus, the specific hydrogen bond cluster at the bottom of TM3 and TM6 was conserved in the D3 receptor.

## DISCUSSION

Although the D3 receptor is an essential target to treat nervous system disorders, its literal 3D structure is unavailable, and the structural basis of the agonist binding to D3 is poorly understood. Here, we systematically studied the important chemical features of potent D3 agonists, the binding mode of an agonist in the D3 receptor, and the induced effect of D3 caused by an agonist, which can contribute to improve our understanding of the agonist binding to the D3 receptor and might be exploited in further drug discovery efforts. Remarkably, we set the D3 agonist pharmacophore as a standard to choose a reasonable 3D structure model of D3 for the

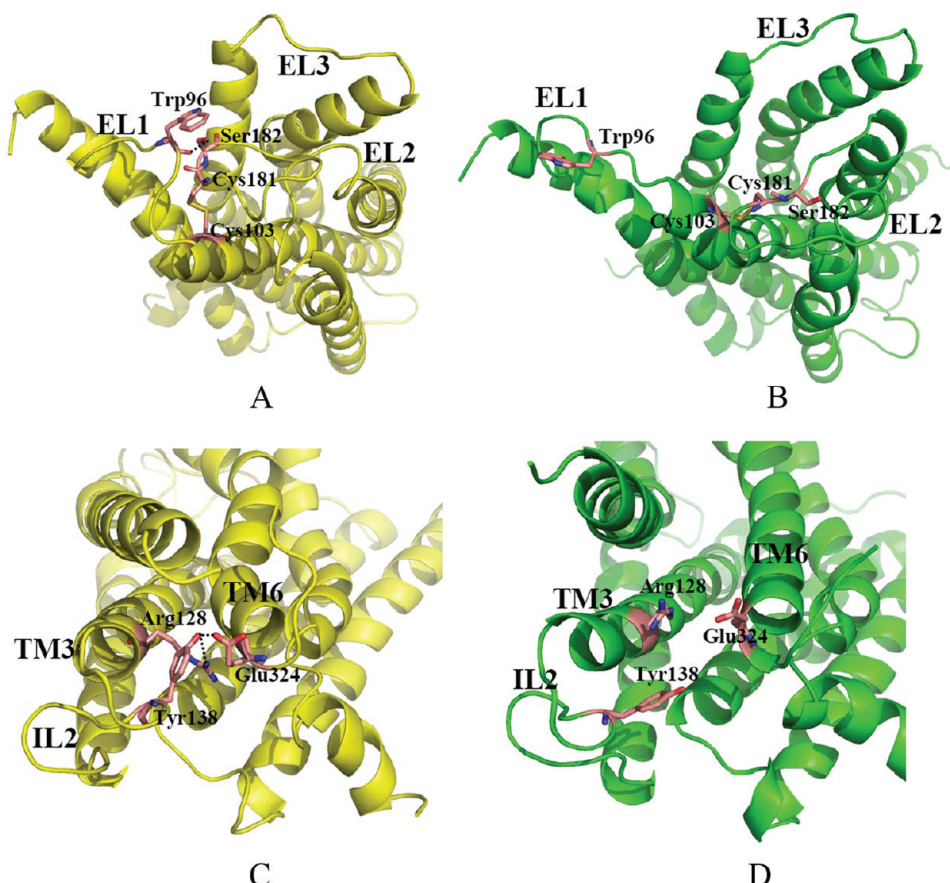


**Figure 6.** Extracellular and intracellular comparison of the D3 receptors in both free D3 and D3–compound 19 simulation systems. (A) Extracellular structure of D3 receptor at 10 ns in the free D3 simulation system. (B) Extracellular structure of D3 receptor at 10 ns in the D3–compound 19 simulation system. (C) Intracellular structure of D3 receptor at 10 ns in the free D3 simulation system. (D) Intracellular structure of D3 receptor at 10 ns in the D3–compound 19 simulation system. The D3 receptors are shown in cartoon, and the side chains of crucial interaction are shown in stick and labeled.

following simulations, employed QSAR-like approach to investigate the rationality of compound 19 binding to D3, and also proposed the signal transduction mechanism of the D3 receptor.

The D2 receptor has different states before and after agonist binding,<sup>63</sup> and maybe the D3 receptor, a D2-like receptor, possesses the similar conformational change. To construct the D3–compound 19 complex, we first built the 3D models of D3 by homology modeling and then identified the correct D3 structure model carefully. Considering that the active-state D3 structure should accord with the important chemical features of the D3 agonists, the D3 agonist pharmacophore hypothesis was built based on 18 diverse D3 agonists, and it was used as criteria to identify the correct D3 model. The 3D structure model of the D3 receptor that accorded with the pharmacophore model best was chosen to construct the D3–compound 19 complex used as the starting structure for the following MD simulations. After inversely scanning the three structures, the inactive and active states of D3 and the starting structure for the MD simulations of D3, we amazingly found that the selected starting structure of D3 was much similar to the active state D3. In the starting structure of D3, not only Ser182 in EL2 was far away from residue Trp96, and accordingly the extracellular “door” was open, but also the intracellular “ionic lock” was turned on to wait for the upriver activation signal and to transduce it to downstream. Therefore, the pharmacophore hypothesis

could be a favorable criterion to identify the reasonable modeling structure for further drug designs.

To reproduce the “actual” binding pose of compound 19 in D3 receptor, we used a QSAR-like analysis for the initial docking conformation selection. First, we docked compound 19 and its analogues to the D3 receptor and predicted their binding energies, and then we compared their predicted binding energies and the experimental values to evaluate the reliability of the homology model and the binding poses from the molecular docking studies. This method helps to not only inspect if the docking method is suitable to our system but also to check the docked binding mode. In our study, the correlation between the predicted binding energies and the experimental values had a good conventional correlation, indicating that the docking method we used could have a high reliability in producing the binding mode for compound 19 in D3 receptor, and the built D3–compound 19 complex was reasonable for the following MD simulations. And the binding mode of compound 19 in D3 was also supported by the experimental mutation data discussed in the Results Section.

Based on our MD simulations, the binding of compound 19 to D3 leads to obvious conformational change compared with the free D3. The agonist binding not only induced D3 to have greater rotary motion in the membrane, especially for TM3 and TM7, but also resulted in the moving away of EL2 from the outside of the membrane to expose the D3

binding site and the disappearance of the hydrogen bonds between residues Arg128, Glu324, and Tyr138 from the inside of the membrane. From the MD simulations, we supposed the signal transduction mechanism of the D3 receptor. EL2 of the D3 receptor might act as a “door” in its activation process. The door is closed when D3 is in the inactive state to protect its binding active site. And when ligand binds to the active site, the door is open. Accompanying the closing and opening of the door, the disulfide bond participated by EL2 (between residues Cys181 and Cys103) rotated about 90 degree (Figure 6). As for the “ionic lock” located in the inside of the D3 receptor, it might act as the transductant of the activation signal. It is locked through hydrogen bonds when D3 is in its inactive state, and it is unlocked when the agonist is binding to D3. Accordingly, the activation process of the D3 receptor was proposed as following: the “door”, acted by EL2, opens for agonist binding to the active site, and the “ionic lock” disrupts to transduce the activation signal from the extracellular to the intracellular. This supposition was supported by the accepted postulate about the activation of GPCRs.<sup>64,65</sup>

## CONCLUSIONS

The dopamine 3 (D3) receptor is a promising therapeutic target for a variety of conditions, including schizophrenia, Parkinson’s disease, and depression. However, it remains challenging to develop potent D3 receptor agonists. Here, we investigated the D3 receptor by employing a computational method aiming to provide useful guidance in the discovery/design of potent D3 receptor agonists.

In this study, a pharmacophore model of D3 receptor agonists was built based on 18 structurally diverse compounds. Our pharmacophore model consists of one positively ionized charge feature, one hydrogen-bond donor feature, one excluded volume feature, and two hydrophobic points. This model gave molecular structure features required in potent D3 receptor agonists. It should be helpful in selecting novel lead compounds with improved activity in three-dimensional (3D) database screenings and useful for designing novel D3 agonists started with the leads. Our 3D structure of the D3 receptor was generated based on the template of the highest homologous protein crystal structure,  $\beta$ 2AD. On the one hand, the modeled 3D structure was used to identify the important residues for the binding between D3 and ligands by analyzing the interactions between compound 19 and D3. On the other hand, it was used to investigate the induced fit effects of D3 by the agonist binding and to obtain an active-state D3 structure which can be used for discovering new scaffold compounds targeting the D3 receptor through 3D database screening. The detailed mechanism at the molecular level of the D3 agonistic action of agonist was also delineated. Our models indicated that the long and flexible EL2 might act as a “door” for agonist binding and that the “ionic lock” at the bottom of TM3 and TM6 might act to transduce the activation signal. Taken together, the agonist binding on the D3 receptor was investigated here, and the information from this paper would be helpful for the future discovery/design of novel D3 agonists.

## ACKNOWLEDGMENT

We thank Prof. Shaomeng Wang in University of Michigan for fruitful discussions on pharmacophore-guided ho-

mology modeling and QSAR-based docking. This work was supported in part by grants from National Natural Science Foundation of China (20702009), Shanghai PuJiang Program (10PJ1406800), National Natural Science Foundation of China (90919021), Innovation Program of Shanghai Municipal Education Commission (09ZZ23), and the Key Project of Chinese Ministry of Education (109060).

**Supporting Information Available:** Chemical structures of the 18 training set molecules (Figure S1) and plot of their actual  $K_i$  versus estimated  $K_i$  (Figure S2), plot of the actual binding energy versus estimated binding energy of our D3 agonist/partial agonist set (Figure S3), and the RMSD (Figure S4) and RMSF (Figure S5) values of D3 from both simulation systems. This information is available free of charge via the Internet at <http://pubs.acs.org>.

## REFERENCES AND NOTES

- (1) Sokoloff, P.; Giros, B.; Martres, M. P.; Bouthenet, M. L.; Schwartz, J. C. Molecular cloning and characterization of a novel dopamine receptor (D3) as a target for neuroleptics. *Nature* **1990**, *347*, 146–151.
- (2) Landwhermeyer, B.; Mengod, G.; Palacios, J. M. Dopamine D3 receptor mRNA and binding sites in human brain. *Mol. Brain Res.* **1993**, *18*, 187–192.
- (3) Murray, A. M.; Ryoo, H. L.; Gurevich, E.; Joyce, J. N. Localization of dopamine D3 receptors to mesolimbic and D2 receptors to mesostriatal regions of human forebrain. *Proc. Natl. Acad. Sci. U.S.A.* **1994**, *91*, 11271–11275.
- (4) Bouthenet, M. L.; Souil, E.; Martres, M. P.; Sokoloff, P.; Giros, B.; Schwartz, J. C. Localization of dopamine D3 receptor mRNA in the rat brain using in situ hybridization histochemistry: comparison with dopamine D2 receptor mRNA. *Brain Res.* **1991**, *564*, 203–219.
- (5) Joyce, J. N.; Millan, M. J. Dopamine D3 receptor agonists for protection and repair in Parkinson’s disease. *Curr. Opin. Pharmacol.* **2007**, *7*, 100–105.
- (6) Wustrow, D. J.; Wise, L. D.; Cody, D. M.; MacKenzie, R. G.; Georgic, L. M.; Pugsley, T. A.; Heffner, T. G. Studies of the active conformation of a novel series of benzamide dopamine D2 agonists. *J. Med. Chem.* **1994**, *37*, 4251–4257.
- (7) Bettinetti, L.; Schlotter, K.; Hubner, H.; Gmeiner, P. Interactive SAR studies: rational discovery of super-potent and highly selective D3 receptor antagonists and partial agonists. *J. Med. Chem.* **2002**, *45*, 4594–4597.
- (8) Hobrath, J. V.; Wang, S. Computational elucidation of the structural basis of ligand binding to the dopamine 3 receptor through docking and homology modeling. *J. Med. Chem.* **2006**, *49*, 4470–4476.
- (9) Palczewski, K.; Kumakawa, T.; Hori, T.; Behnke, C. A.; Motoshima, H.; Fox, B. A.; Trong, I. L.; Teller, D. C.; Okada, T.; Stenkamp, R. E.; Yamamoto, M.; Miyano, M. Crystal structure of rhodopsin: a G protein-coupled receptor. *Science* **2000**, *289*, 739–745.
- (10) Varady, J.; Wu, X.; Fang, X.; Min, J.; Hu, Z.; Levant, B.; Wang, S. Molecular modeling of the three-dimensional structure of dopamine 3 (D3) subtype receptor: discovery of novel and potent D3 ligands through a hybrid pharmacophore- and structure-based database searching approach. *J. Med. Chem.* **2003**, *46*, 4377–4392.
- (11) Cherezov, V.; Rosenbaum, D. M.; Hanson, M. A.; Rasmussen, S. G.; Thian, F. S.; Kobilka, T. S.; Choi, H. J.; Kuhn, P.; Weis, W. I.; Kobilka, B. K.; Stevens, R. C. High-resolution crystal structure of an engineered human beta2-adrenergic G protein-coupled receptor. *Science* **2007**, *318*, 1258–1265.
- (12) Rasmussen, S. G.; Choi, H. J.; Rosenbaum, D. M.; Kobilka, T. S.; Thian, F. S.; Edwards, P. C.; Burghammer, M.; Ratnala, V. R.; Sanishvili, R.; Fischetti, R. F.; Schertler, G. F.; Weis, W. I.; Kobilka, B. K. Crystal structure of the human beta2 adrenergic G-protein-coupled receptor. *Nature* **2007**, *450*, 383–387.
- (13) Oliveira, L.; Paiva, A. C. M.; Vriend, G. A common motif in G-protein-coupled seven transmembrane helix receptors. *J. Comput.-Aided Mol. Des.* **1993**, *7*, 649–658.
- (14) Hsieh, G. C.; Hollingsworth, P. R.; Martino, B.; Chang, R.; Terranova, M. A.; O’Neill, A. B.; Lynch, J. J.; Moreland, R. B.; Donnelly-Roberts, D. L.; Kolasa, T.; Mikusa, J. P.; McVey, J. M.; Marsh, K. C.; Sullivan, J. P.; Brioni, J. D. Central mechanisms regulating penile erection in conscious rats: the dopaminergic systems related to the proerectile effect of apomorphine. *J. Pharmacol. Exp. Ther.* **2004**, *308*, 330–338.

- (15) Lenz, C.; Boeckler, F.; Hubner, H.; Gmeiner, P. Analogues of FAUC 73 revealing new insights into the structural requirements of nonaromatic dopamine D3 receptor agonists. *Bioorg. Med. Chem.* **2004**, *12*, 113–117.
- (16) Leopoldo, M.; Berardi, F.; Colabufo, N. A.; De Giorgio, P.; Lacivita, E.; Perrone, R.; Tortorella, V. Structure-affinity relationship study on N-[4-(4-arylpiperazin-1-yl)butyl]arylcarboxamides as potent and selective dopamine D(3) receptor ligands. *J. Med. Chem.* **2002**, *45*, 5727–5735.
- (17) Bergauer, M.; Hubner, H.; Gmeiner, P. Practical ex-chiral-pool methodology for the synthesis of dopaminergic tetrahydroindoles. *Tetrahedron* **2004**, *60*, 1197–1204.
- (18) Lenz, C.; Haubmann, C.; Hubner, H.; Boeckler, F.; Gmeiner, P. Fancy bioisosteres: synthesis and dopaminergic properties of the endiyne FAUC 88 as a novel non-aromatic D3 agonist. *Bioorg. Med. Chem.* **2005**, *13*, 185–191.
- (19) Pugsley, T. A.; Davis, M. D.; Akunne, H. C.; MacKenzie, R. G.; Shih, Y. H.; Damsma, G.; Wikstrom, H.; Whetzel, S. Z.; Georgic, L. M.; Cooke, L. W. Neurochemical and functional characterization of the preferentially selective dopamine D3 agonist PD 128907. *J. Pharmacol. Exp. Ther.* **1995**, *275*, 1355–1366.
- (20) Ennis, M. D.; Stjernlöf, P.; Hoffman, R. L.; Ghazal, N. B.; Smith, M. W.; Svensson, K.; Wikström, H.; Haadsma-Svensson, S. R.; Lin, C. H. Structure-activity relationships in the 8-amino-6,7,8,9-tetrahydro-3H-benz[e]indole ring system: 2. Effects of 8-aminonitrogen substitution on serotonin receptor binding and pharmacology. *J. Med. Chem.* **1995**, *38*, 2217–2230.
- (21) Millan, M. J.; Peglion, J. L.; Vian, J.; Rivet, J. M.; Brocco, M.; Gobert, A.; Newman-Tancredi, A.; Dacquet, C.; Bervoets, K.; Girardon, S. Functional correlates of dopamine D3 receptor activation in the rat *in vivo* and their modulation by the selective antagonist, (+)-S 14297: 1. Activation of postsynaptic D3 receptors mediates hypothermia, whereas blockade of D2 receptors elicits prolactin secretion and catalepsy. *J. Pharmacol. Exp. Ther.* **1995**, *275*, 885–898.
- (22) Chen, J.; Collins, G. T.; Zhang, J.; Yang, C. Y.; Levant, B.; Woods, J.; Wang, S. Design, Synthesis and Evaluation of a Potent and Selective Ligand for the Dopamine 3 (D3) Receptor with a Novel In vivo Behavioral Profile. *J. Med. Chem.* **2008**, *51*, 5905–5908.
- (23) Damsma, G.; Bottema, T.; Westerink, B. H.; Tepper, P. G.; Dijkstra, D.; Pugsley, T. A.; MacKenzie, R. G.; Heffner, T. G.; Wikström, H. Pharmacological aspects of R-(+)-7-OH-DPAT, a putative dopamine D3 receptor ligand. *Eur. J. Pharmacol.* **1993**, *249*, R9–R10.
- (24) Fears, R. B. *Use of indolone derivatives for the treatment of memory disorders, sexual dysfunction and Parkinson's disease*. WO 9323035, 1993.
- (25) Stemp, G.; Ashmeade, T.; Branch, C. L.; Hadley, M. S.; Hunter, A. J.; Johnson, C. N.; Nash, D. J.; Thewlis, K. M.; Vong, A. K.; Austin, N. E.; Jeffrey, P.; Avenell, K. Y.; Boyfield, I.; Hagan, J. J.; Middlemiss, D. N.; Reavill, C.; Riley, G. J.; Routledge, C.; Wood, M. Design and synthesis of trans-N-[2-(6-cyano-1,2,3,4-tetrahydroisoquinolin-2-yl)ethyl]cyclohexyl]-4-quinolinicarboxamide (SB-277011): a potent and selective dopamine D(3) receptor antagonist with high oral bioavailability and CNS penetration in the rat. *J. Med. Chem.* **2000**, *43*, 1878–1885.
- (26) *Discovery Studio*, Accelrys, Inc. San Diego, CA, 2005.
- (27) Smellie, A.; Teig, S. L.; Towbin, P. Poling: Promoting conformational variation. *J. Comput. Chem.* **1995**, *16*, 171–187.
- (28) Brooks, B. R.; Brucolieri, R. E.; Olafson, B. D.; States, D. J.; Swaminathan, S.; Karplus, M. CHARMM: A program for macromolecular energy, minimization, and dynamics calculations. *J. Comput. Chem.* **1983**, *4*, 187–217.
- (29) Steindl, T.; Langer, T. Influenza virus neuraminidase inhibitors: generation and comparison of structure-based and common feature pharmacophore hypotheses and their application in virtual screening. *J. Chem. Inf. Comput. Sci.* **2004**, *44*, 1849–1856.
- (30) Sali, A.; Blundell, T. L. Comparative protein modelling by satisfaction of spatial restraints. *J. Mol. Biol.* **1993**, *234*, 779–815.
- (31) Javitch, J. A.; Fu, D.; Chen, J.; Karlin, A. Mapping the binding-site crevice of the dopamine D2 receptor by the substituted-cysteine accessibility method. *Neuron* **1995**, *14*, 825–831.
- (32) Jones, G.; Willett, P.; Glen, R. C.; Leach, A. R.; Taylor, R. Development and validation of a genetic algorithm for flexible docking. *J. Mol. Biol.* **1997**, *267*, 727–748.
- (33) Wang, R.; Lai, L.; Wang, S. Further development and validation of empirical scoring functions for structure-based binding affinity prediction. *J. Comput.-Aided Mol. Des.* **2002**, *16*, 11–26.
- (34) Cheng, T.; Li, X.; Li, Y.; Liu, Z.; Wang, R. Comparative assessment of scoring functions on a diverse test set. *J. Chem. Inf. Model.* **2009**, *49*, 1079–1093.
- (35) Berendsen, H. J. C.; Spoel, V. D.; Drunen, R. V. GROMACS: a message-passing parallel molecular dynamics implementation. *Comput. Phys. Commun.* **1995**, *95*, 43–56.
- (36) Van Aalten, D. M. F.; Bywater, R.; Findlay, J. B. C.; Hendlich, M.; Hooft, R. W. W.; Vriend, G. PRODRG, a program for generating molecular topologies and unique molecular descriptors from coordinates of small molecules. *J. Comput.-Aided Mol. Des.* **1996**, *10*, 255–262.
- (37) Breneman, C. M.; Wiberg, K. B. Determining atom-centered monopoles from molecular electrostatic potentials. *J. Comput. Chem.* **1990**, *11*, 361–397.
- (38) Frisch, M. J.; Trucks, G. W.; Schlegel, H. B.; Scuseria, G. E.; Robb, M. A.; Cheeseman, J. R.; Scalmani, G.; Barone, V.; Mennucci, B.; Petersson, G. A.; Nakatsuji, H.; Caricato, M.; Li, X.; Hratchian, H. P.; Izmaylov, A. F.; Bloino, J.; Zheng, G.; Sonnenberg, J. L.; Hada, M.; Ehara, M.; Toyota, K.; Fukuda, R.; Hasegawa, J.; Ishida, M.; Nakajima, T.; Honda, Y.; Kitao, O.; Nakai, H.; Vreven, T.; Montgomery, J. A., Jr.; Peralta, J. E.; Ogliaro, F.; Bearpark, M.; Heyd, J. J.; Brothers, E.; Kudin, K. N.; Staroverov, V. N.; Kobayashi, R.; Normand, J.; Raghavachari, K.; Rendell, A.; Burant, J. C.; Iyengar, S. S.; Tomasi, J.; Cossi, M.; Rega, N.; Millam, N. J.; Klene, M.; Knox, J. E.; Cross, J. B.; Bakken, V.; Adamo, C.; Jaramillo, J.; Gomperts, R.; Stratmann, R. E.; Yazyev, O.; Austin, A. J.; Cammi, R.; Pomelli, C.; Ochterski, J. W.; Martin, R. L.; Morokuma, K.; Zakrzewski, V. G.; Voth, G. A.; Salvador, P.; Dannenberg, J. J.; Dapprich, S.; Daniels, A. D.; Farkas, Ö.; Foresman, J. B.; Ortiz, J. V.; Cioslowski, J.; Fox, D. J. *Gaussian* 98, revision A.7; Gaussian, Inc.: Pittsburgh, PA., 1998.
- (39) Efremov, R. G.; Nolde, D. E.; Vergoten, G.; Arseniev, A. S. A solvent model for simulations of peptides in bilayers. II. Membrane-spanning R-helices. *Biophys. J.* **1999**, *76*, 2460–2471.
- (40) Heller, H.; Schaefer, M.; Schulten, K. Molecular dynamics simulation of a bilayer of 200 lipids in the gel and in the liquid-crystal phases. *J. Phys. Chem.* **1993**, *97*, 8343–8360.
- (41) Berendsen, H. J. C.; Postma, J. P. M.; Gunsteren, W. F.; Dinola, A.; Haak, J. R. Molecular dynamics with coupling to an external bath. *J. Chem. Phys.* **1984**, *81*, 3684–3690.
- (42) Hess, B.; Bekker, H.; Berendsen, H. J. C.; Fraaije, J. G. E. M. LINCS: a linear constraint solver for molecular simulations. *J. Comput. Chem.* **1997**, *18*, 1463–1472.
- (43) Darden, T.; York, D.; Pedersen, L. Particle mesh Ewald: an  $N \cdot \log(N)$  method for Ewald sums in large systems. *J. Chem. Phys.* **1997**, *98*, 10089–10092.
- (44) Boeckler, F.; Gmeiner, P. Dopamine D3 receptor ligands: recent advances in the control of subtype selectivity and intrinsic activity. *Biochim. Biophys. Acta* **2007**, *1768*, 871–887.
- (45) Boeckler, F.; Gmeiner, P. The structural evolution of dopamine D3 receptor ligands: structure-activity relationships and selected neuropsychological aspects. *Pharmacol. Ther.* **2006**, *112*, 281–333.
- (46) Hübner, H.; Haubmann, C.; Utz, W.; Gmeiner, P. Conjugated enynes as nonaromatic catechol bioisosteres: synthesis, binding experiments, and computational studies of novel dopamine receptor agonists recognizing preferentially the D(3) subtype. *J. Med. Chem.* **2000**, *43*, 756–762.
- (47) van Leeuwen, D. H.; Eisenstein, J.; O'Malley, K.; MacKenzie, R. G. Characterization of a chimeric human dopamine D3/D2 receptor functionally coupled to adenylyl cyclase in Chinese hamster ovary cells. *Mol. Pharmacol.* **1995**, *48*, 344–351.
- (48) Filteau, F.; Veilleux, F.; Levesque, D. Effects of reciprocal chimeras between the C-terminal portion of third intracellular loops of the human dopamine D2 and D3 receptors. *FEBS Lett.* **1999**, *447*, 251–256.
- (49) Shi, L.; Simpson, M. M.; Ballesteros, J. A.; Javitch, J. A. The first transmembrane segment of the dopamine D2 receptor: Accessibility in the binding site crevice and position in the transmembrane bundle. *Biochemistry* **2001**, *40*, 12339–12348.
- (50) Javitch, J. A.; Fu, D.; Chen, J. Residues in the fifth membrane-spanning segment of the dopamine D2 receptor exposed in the binding-site crevice. *Biochemistry* **1995**, *34*, 16433–16439.
- (51) Javitch, J. A.; Fu, D.; Chen, J. Differentiating dopamine D2 ligands by their sensitivities to modification of the cysteine exposed in the binding-site crevice. *Mol. Pharmacol.* **1996**, *49*, 692–698.
- (52) Javitch, J. A.; Ballesteros, J. A.; Weinstein, H.; Chen, J. A cluster of aromatic residues in the sixth membrane-spanning segment of the dopamine D2 receptor is accessible in the binding-site crevice. *Biochemistry* **1998**, *37*, 998–1006.
- (53) Javitch, J. A.; Ballesteros, J. A.; Chen, J.; Chiappa, V.; Simpson, M. M. Electrostatic and aromatic microdomains within the binding-site crevice of the D2 receptor: contributions of the second membrane-spanning segment. *Biochemistry* **1999**, *38*, 7961–7968.
- (54) Javitch, J. A.; Shi, L.; Simpson, M. M.; Chen, J.; Chiappa, V.; Visiers, I.; Weinstein, H.; Ballesteros, J. A. The fourth transmembrane segment of the dopamine D2 receptor: accessibility in the binding-site crevice and position in the transmembrane bundle. *Biochemistry* **2000**, *39*, 12190–12199.
- (55) Fu, D.; Ballesteros, J. A.; Weinstein, H.; Chen, J.; Javitch, J. A. Residues in the seventh membrane-spanning segment of the dopamine

- D2 receptor accessible in the binding-site crevice. *Biochemistry* **1996**, *35*, 11278–11285.
- (56) Alberts, G. L.; Pregenzer, J. F.; Im, W. B. Br. Contributions of cysteine 114 of the human D3 dopamine receptor to ligand binding and sensitivity to external oxidizing agents. *J. Pharmacol.* **1998**, *125*, 705–710.
- (57) Sartania, N.; Strange, P. G. Role of conserved serine residues in the interaction of agonists with D3 dopamine receptors. *J. Neurochem.* **1999**, *72*, 2621–2624.
- (58) Lundstrom, K.; Turpin, M. P.; Large, C.; Robertson, G.; Thomas, P.; Lewell, X. Q. Mapping of dopamine D3 receptor binding site by pharmacological characterization of mutants expressed in CHO cells with the Semliki Forest virus system. *J. Recept. Signal Transduction Res.* **1998**, *18*, 133–150.
- (59) Mansour, A.; Meng, F.; Meador-Woodruff, J. H.; Taylor, L. P.; Civelli, O.; Akil, H. Site-directed mutagenesis of the human dopamine D2 receptor. *Eur. J. Pharmacol.* **1992**, *227*, 205–214.
- (60) Cho, W.; Taylor, L. P.; Mansour, A.; Akil, H. Hydrophobic residues of the D2 dopamine receptor are important for binding and signal transduction. *J. Neurochem.* **1995**, *65*, 2105–2115.
- (61) Daniell, S. J.; Strange, P. G.; Naylor, L. H. Site-directed mutagenesis of Tyr417 in the rat D2 dopamine receptor. *Biochem. Soc. Trans.* **1994**, *22*, 144S.
- (62) Ballesteros, J. A.; Jensen, A. D.; Liapakis, G.; Rasmussen, S. G. F.; Shi, L.; Gether, U.; Jonathan, J. A. Activation of the b2-adrenergic receptor involves disruption of an ionic lock between the cytoplasmic ends of transmembrane segments 3 and 6. *J. Biol. Chem.* **2001**, *276*, 29171–29177.
- (63) Fu, W.; Shen, J.; Luo, X.; Zhu, W.; Cheng, J.; Yu, K.; Briggs, J. M.; Jin, G.; Chen, K.; Jiang, H. Dopamine D1 receptor agonist and D2 receptor antagonist effects of the natural product (-)-stepholidine: molecular modeling and dynamics simulations. *Biophys. J.* **2007**, *93*, 1431–1441.
- (64) González-Maeso, J.; Sealfon, S. C. Agonist-trafficking and hallucinogens. *Curr. Med. Chem.* **2009**, *16*, 1017–1027.
- (65) Iwasiorw, R. M.; Nantel, M. F.; Tiberi, M. Delineation of the structural basis for the activation properties of the dopamine D1 receptor subtypes. *J. Biol. Chem.* **1999**, *274*, 31882–31890.

CI1002119